

Polar ordering of smectic liquid crystals within the interfacial region

M. Harke, M. Ibn-Elhaj, H. Möhwald, and H. Motschmann*

Max-Planck-Institute of Colloids and Interfaces, Rudower Chaussee 5, D-12489 Berlin, Germany

(Received 16 July 1997)

The triblock organosiloxane liquid crystalline 4-(pentamethyl-disiloxanyl-*n*-pentyloxy)-4'-cyanodiphenyl, which forms a smectic S_A phase in the bulk, was investigated at the air-water interface. Imaging null ellipsometry was employed for visualization of morphology and thickness determination. The surface pressure-area (π - A) isotherm exhibits several plateaus, each corresponding to the formation of an interdigitated bilayer. The system is ideally suited for assessment of the influence of the interface on the order and structure of the smectic bulk phase. By further compression all subsequently formed bilayers are of identical thickness and the value matches the layer spacing of the S_A phase. Despite these apparent similarities, deviations between bulk and interfacial regions were revealed by optical second-harmonic generation. In contrast to the bulk, the first and second bilayers contain an excess of dipoles as well as molecules with tilt. The transition region between the bulk and interface is composed of at least two bilayers. The findings were further verified by surface potential measurements. [S1063-651X(98)13002-7]

PACS number(s): 61.30.-v

I. INTRODUCTION

Liquid crystals are fluid systems that respond to slight changes in applied external forces [1]. This feature makes them attractive for many applications, e.g., in displays. In this respect, one important, but still not completely understood process, is the way in which liquid crystals are anchored to an interface and how this interfacial order effects the volume phase [2]. The presence of a transition (interface-bulk) region seems to be a common feature of nematic liquid crystals and is confirmed by a great body of experimental evidence. However, smectic liquid crystals (layer structures) seem to lack this features [3]. Our present contribution focuses in particular on this aspect.

Among the established surface analytical tools, second-harmonic generation (SHG) is ideally suited to retrieve information on the orientation of the interfacial region as well as identification of its symmetry [4,5]. Many liquid crystals possess conjugated π systems with a high second-order hyperpolarizability β . When oriented they contribute to strong SHG signals and data analysis is drastically simplified since the molecular hyperpolarizability tensor is usually dominated by a single component β_{zzz} in the direction of the π system.

SHG was used to determine the orientation of the liquid-crystal 4'-*n*-alkyl-4-cyanobiphenyl in the interfacial regions and these findings were correlated with the orientational order of the bulk [6]. Freely suspended films of the smectic phase S_A of 4'-*n*-octyl-4-cyanobiphenyl (8CB) were also investigated by SHG [7]. The SHG signal versus the layer number N could be approximated by a straight line through the origin and no deviations for small layer numbers were observed. Therefore, it could be concluded that a freely suspended film consists of layers identical in structure to those in the S_A bulk phase where an interdigitated bilayer with an antiparallel molecular arrangement was identified. Due to the

molecular arrangement the dipole contribution to the SHG signal vanishes and thus the SHG signal is only made up of its weak quadrupole contribution.

Deposited on glass [8] or water [9], the very same liquid crystal forms initially a monolayer with tilt. The SHG analysis for a thick film ($\geq 100 \mu\text{m}$) turned out to be fairly complex since the quadrupole contribution of the bulk phase has to be separated from the dipole contribution of the monolayer. The quadrupole contribution to the polarizability is about a factor of 1000 weaker than the dipole contribution, but it scales with the number of molecules. As a result, both can be of the same order. Due to a phase shift of π between both contributions, the observed SHG signal of a thick film is weaker than the monolayer signal. Ultrathin layers of 8CB at the air-water interface have been investigated by Xue *et al.* [10]. They observed a strong decrease in the SHG signal during the formation of the first bilayer on top of the monolayer. These findings were also explained in terms of a quadrupole contribution of the bilayer. This interpretation appears to be puzzling since a simple estimation reveals that both should be orders of magnitude apart.

The difference in the structure of a freely suspended film and one deposited on a glass slide or formed at the air-water interface can be understood. With the latter the polar head group is preferentially attached to the polar substrate and as a result an oriented monolayer with tilt is formed. According to the data available, all bilayers of 8CB in the vicinity of the interface possess properties similar to the volume phase. In this contribution these findings are assessed; instead of 8CB a related compound is used that forms during compression several stable multilayers at the air-water interface. This system is one of the smectic liquid crystals that form stable multilayers at the air-water interface before a transition to a three-dimensional phase [11,12]. In addition, the system shows only a little hysteresis. The thickness, orientation, symmetry, and morphology in the arrangement is retrieved from *in situ* SHG and imaging null ellipsometry measurements [13]. These techniques allow a step by step investigation of the influence of the interface. Complications in data

*Author to whom correspondence should be addressed. Electronic address: motschma@mpikg.fta-berlin.de

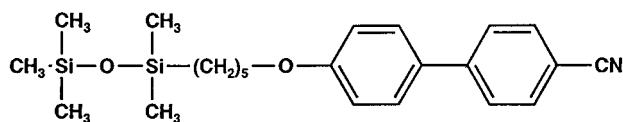


FIG. 1. Chemical structure of the triblock organosiloxane smectogen 4-(pentamethyl-disiloxanyl-*n*-pentyloxy)-4'-cyanodiphenyl used in this study.

analysis arising from strong quadrupole contributions are also avoided.

II. EXPERIMENT

A. Materials

The chemical structure of the amphiphilic liquid-crystal 4-(pentamethyl-disiloxanyl-*n*-pentyloxy)-4'-cyanodiphenyl (5AB) used in this study is given in Fig. 1. The synthesis and purification of the material is described in [14]. The most important structural elements are (i) the mesogenic unit consisting of biphenyl, (ii) the cyano group that anchors it at the air-water interface and ensures in addition a high hyperpolarizability, and (iii) the siloxane block that provides sufficient hydrophobicity and flexibility to prevent crystallization. The peak of the UV-visible absorption band is at 307 nm; SHG was performed off resonance.

B. Langmuir layer

Monolayer film formations were carried out from the pure water subphase with no deliberately added solutes (Milli-Q). The films were prepared on a commercial Langmuir trough purchased from R&K GmbH. The liquid crystal was dissolved in chloroform.

C. Optical characterization

Second-harmonic generation experiments were carried out in reflection mode at a fixed angle of incidence of 53° . The fundamental ($\lambda = 1064$ nm) of an active-passive mode locked Nd:YAG laser (PY-61, Continuum, where YAG denotes yttrium aluminum garnet) with a pulse width of $\tau = 35$ ps and a repetition rate of 12.5 Hz was used as a light source. The beam diameter was adjusted by a telescope to 1.5 mm. All spurious SHG signals created by the optical components were removed by a visible cutoff filter (RG630, Schott) placed just in front of the sample. The frequency-doubled light generated at the interface was separated from the fundamental by an IR-cutoff filter (BG39, Schott) in conjunction with a narrow-band interference filter (532 BP, Instruments S.A.) and subsequently detected by a photomultiplier (C83068, Burle) with a quantum efficiency of 15%. The signal was amplified (V5D, Fa. Seefeldler Meatechnik) and processed by a 500-MHz, 2-GSa/s digitizing oscilloscope (HP 54522 A, Hewlett-Packard). All vital elements of the experiment are computer controlled. In order to eliminate experimental errors due to fluctuations in laser pulse intensity, the SHG signal of a quartz crystal was used as a reference. The plane of polarization of the incident beam can be rotated by a Glan laser polarizer [extinction ratio 10^{-6} (PGL, Halle)] and a low-order quartz half wave plate ($\Delta\lambda = 0.001$, RLQ Halle) mounted in motor driven rotary stage (M-445.21,

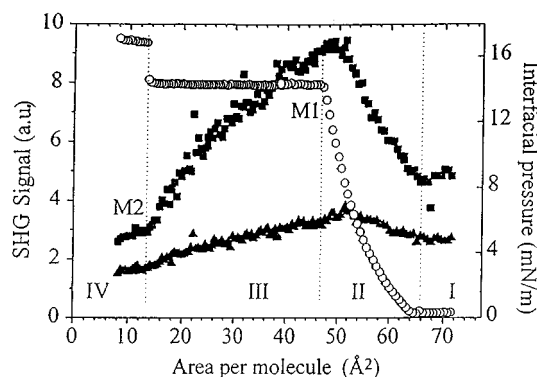


FIG. 2. π -A isotherm (circles) of the liquid-crystal 5AB together with the synchronously measured SHG signal. The π -A isotherm exhibits several plateaus. The triangles refer to a \hat{p} polarization of the incident fundamental beam, whereas the squares refer to an \hat{s} polarization; both were recorded at a fixed analyzer setting of \hat{p} polarization.

Physik Instrumente) equipped with optical encoders. The polarization of the reflected SHG light can be analyzed by means of a Glan-Thomson prism (extinction ratio 10^{-6} , Typ K, Fa. Steeg & Reuter).

Imaging null ellipsometry was carried out using a setup described in detail in [15]. The procedure used for data analysis is described in [16]. All optical characterizations were performed *in situ*.

III. RESULTS AND DISCUSSION

The π -A isotherm of the system is presented in Fig. 2 together with the SHG data as measured in reflection. The squares represent SHG measurements with an \hat{s} polarization of the incident fundamental beam, whereas the triangles refer to a \hat{p} polarization; both were recorded at a fixed analyzer setting of \hat{p} polarization. The system exhibits some unusual features. The π -A isotherm possesses several plateaus. Each corresponds to the coexistence of two phases, which does not reflect a collapse of the system, as might be concluded from apparent similarities with other systems [17]. Careful sample preparation allows the formation of even five bilayers.

Brewster angle microscopy (BAM) has been used elsewhere [18] for visualization of the morphology of the same liquid-crystal system as investigated here. BAM images revealed the formation of circular domains. At the end of a plateau a homogeneous layer is again formed. The thickness of each phase was identified with the aid of x-ray reflectometry [19] and thus a formation of a bilayer on top of a monolayer was verified. Here imaging null ellipsometry [13] was used and both visualization of the morphology and a simultaneous thickness determination could be performed. The lateral resolution is of the order of micrometers as compared to centimeters with x rays. The accuracy in the thickness determination turned out to be comparable. The advantage of this technique is that the optical measurements are fast, nondestructive, and do not require expensive instrumentation.

A null ellipsometric image of the morphology is presented in Fig. 3. The image was recorded in the second plateau of the π -A isotherm. The morphology in all the two-phase regions is quite similar; domains are of circular shape and do

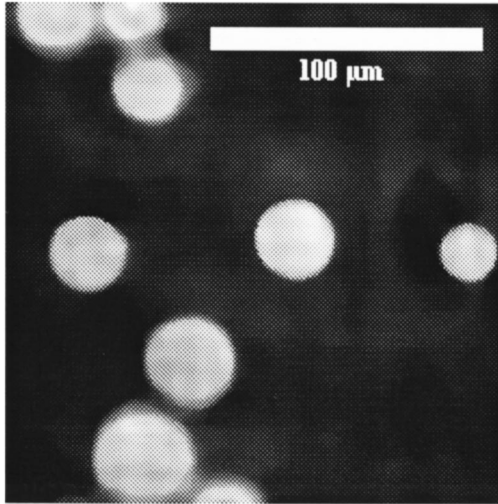


FIG. 3. Visualization of the morphology with the aid of imaging null ellipsometry. The image presented was recorded in the second plateau of the π - A isotherm, but similar features are observed in all two-phase regions. All domains do not exhibit any internal structure and require the same setting of the polarization optics for a complete cancellation of the reflected light. The contrast of all images can be inverted with the compensator setting. The null setting of all domains can be described by a uniaxial layer model assuming a bilayer of thickness of 1.7 of the molecular length and extraordinary and ordinary refractive indices of $n_{\perp} = 1.52$ and $n_{\parallel} = 1.46$, respectively.

not possess any internal structure on the mesoscopic length scale. All domains require the very same extinction setting of the polarization optics in order to achieve a complete cancellation of the light and the contrast in the images can be inverted with the compensator setting. The presence of only two phases is thus verified. The null setting can be modeled using a Fresnel algorithm and a uniaxial layer model. The null setting of all domains can be described by a bilayer of a thickness of 1.7 of the molecular length and by the use of the values $n_{\perp} = 1.52$ and $n_{\parallel} = 1.46$ for the extraordinary and the ordinary refractive index, respectively. All subsequently formed bilayers are of the same thickness. The value matches the layer spacing of the smectic phase where an interdigitated bilayer was identified [18]. The driving force for this structure is the dipole-dipole interaction of the molecules through their cyano end groups. The first monolayer cannot be described by the same set of parameters and possesses different properties.

The above observations are in good agreement with [3], where it is claimed that the transition region of a smectic liquid crystal, in contrast to a nematic crystal, comprises only the first monolayer. Despite apparent similarities between bulk and interfacial region there are striking deviations as revealed by SHG. SHG is determined by the dipole contribution and measures the components of the macroscopic susceptibility tensor $\chi^{(2)}$, which is related to the molecular quantities by the oriented gas model [20]:

$$\chi^{(2)} = \sum_{\text{mol}} \beta = N \langle \beta \rangle. \quad (1)$$

It states that the susceptibility $\chi^{(2)}$ is the sum of the hy-

perpolarizabilities β of all molecules. This can also be expressed in terms of their number density N and their corresponding orientational average $\langle \beta \rangle$ as denoted by the angular brackets. The macroscopic susceptibility tensor $\chi^{(2)}$ is defined in the laboratory frame of reference (I, J, K) as given by the plane of incidence and the hyperpolarizability β is defined in the molecular frame of reference (i, j, k) . Both third-rank tensors can be transformed using a Euler transformation [21]

$$\beta_{IJK} = \mathbf{U}_{Ii}(\phi, \theta, \psi) \beta_{ijk} \mathbf{U}_{Jj}^{-1}(\phi, \theta, \psi) \mathbf{U}_{Kk}^{-1}(\phi, \theta, \psi), \quad (2)$$

with $\mathbf{U} = \mathbf{R}_c \mathbf{R}_b \mathbf{R}_a$ and the \mathbf{R}_i describing the subsequent rotation around three axes a, b, c :

$$\begin{aligned} R_c(\psi) &= \begin{pmatrix} \cos \psi & \sin \psi & 0 \\ -\sin \psi & \cos \psi & 0 \\ 0 & 0 & 1 \end{pmatrix}, \\ R_b(\phi) &= \begin{pmatrix} \cos \phi & \sin \phi & 0 \\ -\sin \phi & \cos \phi & 0 \\ 0 & 0 & 1 \end{pmatrix}; \\ R_a(\theta) &= \begin{pmatrix} \cos \theta & 0 & -\sin \theta \\ 0 & 1 & 0 \\ \sin \theta & 0 & \cos \theta \end{pmatrix}. \end{aligned} \quad (3)$$

Evaluation of these equations is a tedious procedure involving lengthy expressions relating the individual tensor components. The explicit calculation can be found in [22] or can be conveniently generated with the aid of algebraic computer math packages (e.g., MATHEMATICA, Wolfram Research).

From our experimental arrangement these equations are significantly simplified. The chromophore used in this study is dominated by its β_{zzz} component with its value being orders of magnitude greater than any other element of the tensor. Thus the β tensor can be treated as a scalar quantity. In addition, the number of independent tensor elements is further reduced by the symmetry in the arrangement of the molecules. In our experiment a $C_{\infty v}$ symmetry with an isotropic azimuthal distribution of the molecules is observed. The remaining tensor elements are

$$\chi_{zzz} = N \beta_{zzz} \langle \cos^3 \theta \rangle, \quad (4)$$

$$\chi_{xxz} = \chi_{xzx} = \chi_{zxx} = \chi_{yyz} = \chi_{zyy} = 1/2 N \beta_{zzz} \langle \cos \theta \sin^2 \theta \rangle.$$

Thus a SHG analysis allows the determination of the number density and the orientation of the chromophore.

The isotherm can be divided into four parts as indicated in Fig. 2. Each part exhibits strikingly different features in the SHG experiment. Strong fluctuations in the SHG signal are observed in region I. The surface of the sample is not homogeneously covered by a gaseous phase. Instead, patches of liquid crystal are floating on the surface and move in and out of the laser spot driven by convection. The size and distribution of the patches are dependent on the preparation conditions. The SHG signal becomes stable as soon as an onset in the surface pressure π is recorded and a homogeneous monolayer is formed (region II). Monolayer compression is

accompanied by a strong increase in the SHG intensity for selected polarization settings $I^{2\omega}(\hat{p} \Rightarrow \hat{p})$ (triangles) in Fig. 2 and $I^{2\omega}(\hat{s} \Rightarrow \hat{p})$ (squares). The ratio between these quantities is dependent on the prevailing orientational order within the Langmuir film and changes significantly with compression. These findings cannot be explained in terms of the number density N and differs from the constant tilt angle for an 8CB monolayer during compression as reported in [23]. Hence it has to be explained in terms of changes in tilt.

The most accurate determination of the tilt angle can be achieved by a continuous rotation of the plane of polarization P of the incident beam at fixed settings of the analyzer A . With the aid of Maxwell's equations a relation between the intensity $I^{2\omega}$ and I^ω can be derived. For an analyzer setting at \hat{p} the following equation holds:

$$I^{2\omega} = D | (A \cos^2 P + C \sin^2 P) \chi_{zxx}^{(2)} + B \cos^2 P \chi_{zzz}^{(2)} |^2 I(\omega)^2, \quad (5)$$

with

$$A = [F_z(2\omega)F_x(\omega) - 2F_x(2\omega)F_z(\omega)]F_x(\omega)\cos^2 \alpha,$$

$$B = F_z(2\omega)F_z^2(\omega)\sin^2 \alpha,$$

$$C = F_z(2\omega)F_y^2(\omega),$$

$$D = 4 \left(\frac{\mu_0}{\epsilon_0} \right)^{3/2} \omega^2 \tan^2 \alpha,$$

where P is the angle denoting the polarization of the fundamental with respect to the plane of incidence, α is the angle of incidence, μ_0 is the permeability constant, ϵ_0 is the permittivity constant, and F_i is the Fresnel factor as derived by the boundary conditions at the interfaces. The value is determined by the dielectric function of the individual layer and the angle of incidence α . The corresponding equation for an analyzer setting at \hat{s} reads

$$I^{2\omega} = D F_y^2(2\omega)F_y^2(\omega)F_z^2(\omega)\sin^2(2P) |\chi_{yzy}^{(2)}|^2 I(2\omega)^2. \quad (6)$$

The unknown susceptibility components are the fit parameters. Alternatively, the orientation of the molecule can also be determined by two subsequent measurements of the intensity of SHG light for \hat{s} and \hat{p} polarizations of the incident beam. This procedure is faster and was used to record synchronously the orientation during compression:

$$\frac{\langle \cos^3 \theta \rangle}{\langle \cos \theta \sin^2 \theta \rangle} = \frac{\chi_{zzz}}{\chi_{zxx}} = -\frac{A}{2B} \pm \frac{C}{2B} \sqrt{\frac{I^{2\omega}(P=\hat{p})}{I^{2\omega}(P=\hat{s})}}. \quad (7)$$

The correct sign (+ or -) in Eq. (8) can be determined by an additional intensity measurement at a different polarizer setting.

Figure 4 shows a representative measurement of the SHG intensity $I^{2\omega}$ at a surface pressure of $\pi = 10$ mN/m. The polar diagram shows the SHG intensity $I^{2\omega}$ as a function of the plane of polarization P of the fundamental beam. The squares represent the SHG data as measured and the solid line refers to a fit according to Eqs. (6) and (7). Figure 4(a) corresponds to an analyzer setting of $A = \hat{s}$. The absence of

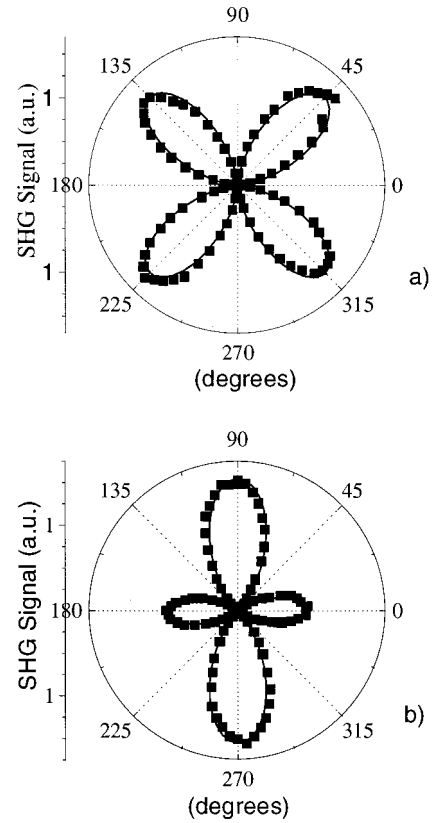


FIG. 4. SHG intensity $I^{2\omega}$ plotted in a polar diagram as a function of the plane of polarization P of the fundamental beam. Squares represent the measured SHG data and the solid line refers to a fit according to Eqs. (7) and (6). (a) An analyzer setting of $A = \hat{s}$. (b) The corresponding data together with the best fit for an analyzer setting at \hat{p} polarization. The measurement was performed in the monolayer region at a surface pressure of $\pi = 10$ mN/m.

second-harmonic light with \hat{s} polarization for \hat{s} or \hat{p} polarization of the fundamental is in agreement with an isotropic azimuthal distribution of the molecules. Figure 4(b) shows the corresponding data together with the best fit for an analyzer setting at \hat{p} polarization. Based on these data and the algorithm described, the orientation within region II of the π -A isotherm can be retrieved. The result is plotted in Fig. 5. Monolayer compression is accompanied by a significant change in the tilt angle of about 8° . A tilt angle of 0° refers to an organization of the molecule parallel to the surface normal.

Region III of the π -A isotherm corresponds to the first coexistence region of a bilayer and monolayer. Surprisingly, the bilayer formation is accompanied by a significant decrease in the recorded SHG intensity. The arrangement of the molecules lead to a partial cancellation of the SHG light. In our experimental arrangement SHG is mainly generated by the dipole contribution of the nonlinear polarization. Higher-order terms of the polarization wave such as quadrupole contributions can be neglected. Experimental evidence of this was provided in [24]. In that paper the SHG intensity of a monolayer was measured and compared to the SHG signal recorded on samples where further molecules from the gas phase have been deposited onto the monolayer. Due to the preparation process, no preferential absolute orientation (up

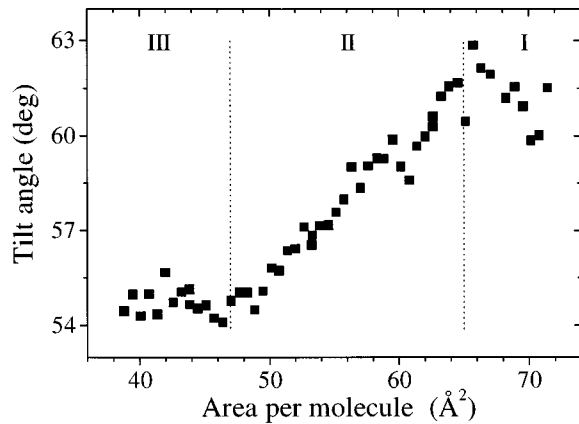


FIG. 5. Tilt angle as a function of the area per molecule. Monolayer compression is accompanied by a significant change in the orientational order. A tilt angle of 0° refers to an upright organization parallel to the surface normal

or down) of the deposited molecules is observed. The experiment detected the first decrease in SHG once the number of deposited molecules exceeded those within the monolayer by a factor of 10.

Therefore, our experimental data can only be explained by dipole contributions within the layer system. Two possibilities that give rise to this are structural changes in the monolayer due to bilayer formation and a SHG signal with a phase shift of π with respect to the monolayer contribution generated by the interdigitated bilayer. The first can be ruled out by a great body of experimental evidence. The features observed in the SHG experiment would require a reduction of the number of molecules N within the monolayer by a factor of 2. Such a dramatic change should also be reflected in the surface tension, which is mainly governed by the first monolayer at the air-water interface. Furthermore, the electron density of the uncovered monolayer matches the value of a monolayer covered with a bilayer according to x-ray measurements [19]. Also changes in the orientational order within the monolayer fail to describe the measurement. Any change in the orientational order is reflected in the ratio of $I^{2\omega}(\hat{p} \Rightarrow \hat{p})/I^{2\omega}(\hat{s} \Rightarrow \hat{p})$ according to Eq. (8). This ratio varies only slightly (from 0.36 to 0.58) corresponding to tilt angles from 54° to 61° , respectively, and is insufficient to account for the observed experimental features. It would lead only to a drop in SHG by a factor of 0.92 as calculated by use of Eqs. (7) and (6). Therefore the experimental observation cannot be described by a monolayer contribution.

Instead, it is evident that the interdigitated bilayer contains an excess of dipoles. The decrease in the signal requires a phase shift of π , which is produced by an upside down orientation of the excess dipoles with respect to the one in the monolayer. Since, in addition, the nonlinear signals $I^{2\omega}$ decrease for both polarizer settings \hat{s} and \hat{p} , the dipoles in the monolayer possess, in addition, a tilt. In the case where the first bilayer would match the organization of the smectic S_A bulk phase ($\theta=0$), all components of the susceptibility tensor despite χ_{zzz} vanish, as is evident from Eq. (5). As a result, the SHG signal $I^{2\omega}(\hat{s} \Rightarrow \hat{p})$ would be independent of the area per molecule as can be readily seen from Eq. (7).

The excess of molecules pointing to the monolayer can be

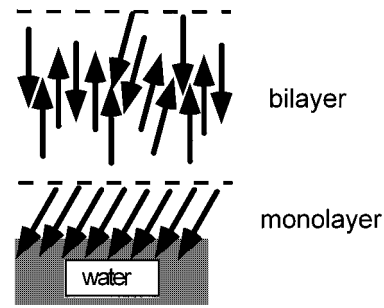


FIG. 6. Schematic representation of the microscopic polar ordering within the layers.

estimated subject to certain simplifying assumptions. Introducing the same dielectric function ϵ for monolayer and bilayer $I^{2\omega}(\hat{s} \Rightarrow \hat{p})$ reads

$$I_{\text{mono}}^{2\omega} = A |\chi_{zxx}^{(2)}|^2 I(\omega)^2, \quad (8)$$

$$I_{\text{bi}}^{2\omega} = A |\chi_{zxx}^{(2)}(M2) - \chi_{zxx}^{(2)}(M1)|^2 I(\omega)^2. \quad (9)$$

The phase difference between both SHG contributions $\exp[ik(\vec{R}_{\text{mono}} - \vec{R}_{\text{bi}})]$ can be neglected since the geometrical distance ($\vec{R}_{\text{mono}} - \vec{R}_{\text{bi}}$) is much smaller than the wavelength. Assuming further the same tilt angle for excess dipoles as observed in the bilayer, one obtains a ratio of excess dipoles pointing opposite to the monolayer dipoles:

$$\delta N = \left(1 - \frac{\sqrt{I_{M1}}}{\sqrt{I_{M2}}} \right) N_{\text{mono}} = 0.44 N_{\text{mono}}. \quad (10)$$

The same feature holds in region IV of the isotherm, but is much less pronounced. Hence the influence of the interface comprises two bilayers.

The microscopic polar ordering is illustrated in Fig. 6. Since our interpretation contradicts that of Xue *et al.* [10], we performed, in addition, surface potential measurements to provide further experimental evidence. The measured surface potential is plotted together with the π -A isotherm in Fig. 7. A significant drop in the surface potential is observed in region III of the isotherm. Detailed and systematic studies and discussions will be given elsewhere. At this stage we

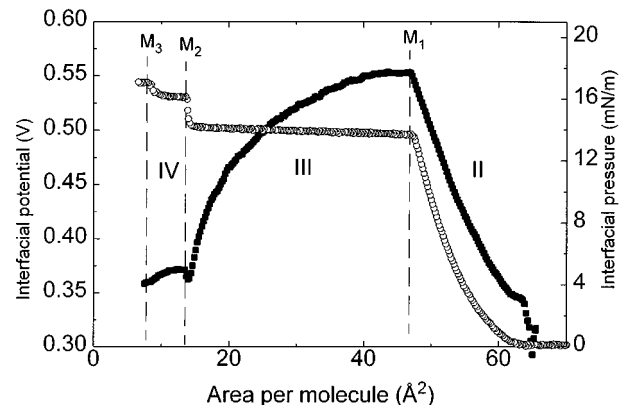


FIG. 7. Surface potential (SP) (squares) and π -A isotherm (triangles). A significant decrease in the SP is observed in region III.

only estimate the excess of dipoles in the bilayer pointing opposite to the monolayer dipoles. The surface potential of the incompressible monolayer (i.e., at point $M1$; see Fig. 7) containing N_{mono} with dipoles pointing down reads, at $M1$,

$$\Delta V_{\text{mono}} \approx 530 \text{ mV}. \quad (11)$$

The surface potential of the three-layer film (i.e., at point $M2$, see Fig. 7) that consist of a bilayer on top of the monolayer reads

$$\Delta V_2 = \Delta V_{\text{mono}} + \Delta V_{\text{bi}} = 350 \text{ mV}. \quad (12)$$

Thus the excess of dipoles pointing up within the bilayer is related to the observed drop in the surface potential according to

$$\frac{N_{\text{bi}}^{\text{up}} - N_{\text{bi}}^{\text{down}}}{N_{\text{mono}}} = \frac{\Delta V_{\text{bi}}}{\Delta V_{\text{mono}}}, \quad (13)$$

which gives

$$N_{\text{bi}}^{\text{up}} - N_{\text{bi}}^{\text{down}} \approx 0.34 N_{\text{mono}}, \quad (14)$$

being in good agreement with the SHG data.

IV. CONCLUSION

A smectogen 5AB anchored at the air-water interface has been investigated. The π -A isotherm possesses a variety of plateaus that correspond to the formation of a bilayer on top of the preformed multilayer. The bilayer gradually adopts the structure of the smectic S_A bulk phase and hence this arrangement allows an assessment of the influence of the interface on the molecular organization in the bulk. Second-harmonic generation was able to reveal, in contrast to the results of surface potential measurements with 8CB [23], a significant change in tilt angle with compression. Furthermore, in analogy to nematic liquid crystals, a transition region between the interfacial layer and the volume phase has been found for smectic liquid crystals. The first and second interdigitated bilayers exhibit significant deviations from the volume phase. They contain an excess of dipoles with an orientation opposite to those in the monolayer. The number of excess dipoles is about 40% of the monolayer dipoles. In contrast to the bulk, there are also tilted molecules in the bilayer.

-
- [1] P. S. Pershan, in *Structure of LC Phases* edited by EDI-TOR(S), Lecture Note in Physics, Vol. 23 (World Scientific, Singapore, 1988).
- [2] H. Knobloch, H. Orendi, M. Blüchel, T. Seki, S. Ito, and W. Knoll, *J. Appl. Opt.* **77**, 481 (1995).
- [3] B. Jérôme, *Rep. Prog. Phys.* **54**, 391 (1991).
- [4] X. Zhao, M. Goh, and K. Eiseenthal, *J. Phys. Chem.* **94**, 2222 (1990).
- [5] Y. R. Shen, *Annu. Rev. Phys. Chem.* **40**, 327 (1989).
- [6] X. Zhuang, L. Marrucci, and Y. R. Shen, *Phys. Rev. Lett.* **73**, 1513 (1994).
- [7] H. Hsiung and Y. R. Shen, *Phys. Rev. A* **34**, 4303 (1986).
- [8] P. Guyot-Sionnest, H. Hsiung, and Y. R. Shen, *Phys. Rev. Lett.* **57**, 2963 (1986).
- [9] C. S. Mullin, P. Guyot-Sionnest, and Y. R. Shen, *Phys. Rev. A* **43**, 6778 (1988).
- [10] J. Xue, C. S. Jung, and W. M. Kim, *Phys. Rev. Lett.* **69**, 474 (1992).
- [11] J. Fang, M. Dennin, Ch. Knobler, Y. Godovsky, N. Makarova, and H. Yokoyama, *J. Phys. Chem. B* **101**, 3147 (1997).
- [12] B. Rapp and H. Gruler, *Phys. Rev. A* **42**, 2215 (1990).
- [13] R. Reiter, H. Motschmann, H. Orendi, A. Nemetz, and W. Knoll, *Langmuir* **8**, 1784 (1992).
- [14] J. Newton, H. Coles, P. Hodge, and J. Hannington, *J. Mater. Chem.* **4**, 869 (1994).
- [15] M. Harke, R. Teppner, O. Schulz, H. Orendi, and H. Motschmann, *Rev. Sci. Instrum.* **68**, 3130 (1997).
- [16] M. Harke, M. Stelzle, and H. Motschmann, *Thin Solid Films* **284**, 412 (1996).
- [17] H. Motschmann, R. Reiter, R. Lawall, G. Wegner, and W. Knoll, *Langmuir* **7**, 2743 (1991).
- [18] M. Ibn-Elhaj, H. Riegler, and H. Möhwald, *J. Phys. I* **6**, 969 (1996).
- [19] M. Ibn-Elhaj, H. Riegler, H. Möhwald, M. Schwendler, and C. A. Helm, *Phys. Rev. E* **56**, 1884 (1997).
- [20] P. Prasad and D. J. Williams, *Introduction to Nonlinear Optical Effects in Molecules and Polymers* (Wiley, New York, 1991).
- [21] H. Goldstein, *Classical Mechanics* (Addison-Wesley, London, 1981).
- [22] C. Hirose, N. Akamatsu, and K. Domen, *Appl. Spectrosc.* **6**, 1051 (1992).
- [23] P. Schmitz and H. Gruler, *Europhys. Lett.* **29**, 451 (1995).
- [24] Y. R. Shen, *Annu. Rev. Phys. Chem.* **40**, 327 (1989).